TENMA OBSERVATIONS OF BRIGHT BINARY X-RAY SOURCES

Hajime Inoue
Institute of Space and Astronautical Science
Komaba, Meguro-ku, Tokyo 153, Japan

ABSTRACT. Spectroscopic study of bright binary X-ray sources, performed with the gas scintillation proportional counters on board Tenma, is reviewed. Properties of an iron emission line from two classes of bright binary X-ray sources: X-ray pulsars and low-mass binary sources, are first presented. It is shown that a most likely candidate for the line emitting region is an Alfven shell in case of X-ray pulsars, whereas that of low mass binary sources is an outer accretion disk. Next, nature of the continuum emission from low-mass binary sources is consistently interpreted by a picture that an optically thick accretion disk extends down to very near the surface of a weakly magnetized neutron star. Origin of ultrasoft spectra of black hole candidate sources is also discussed.

1. INTRODUCTION

Bright close-binary X-ray sources containing neutron stars are generally classified into two groups; X-ray pulsars and non-pulsating low-mass binary X-ray sources. Most of X-ray pulsars have massive primaries of O, B stars, which are distributed along the galactic arms. Hence, these sources are considered to be young systems. On the other hand, low-mass binary sources are distributed preferentially near the galactic center, and are often found within globular clusters. These facts indicate that these sources are old systems. Many of low-mass binary sources produce X-ray bursts, but no X-ray pulsar does. X-ray pulsars are characterized by their pulsation, but no burst source pulsates.

Recent spectroscopic study done with the gas scintillation proportional counters (GSPC) on board Tenma has shown that the properties of an iron emission line from these two classes of sources are also distinctly different. Figure 1 shows pulse-height spectra obtained from typical sources from the two classes; Vela X-1 and Sco X-1. In both of the spectra, two humps are noticeable; one near 5 keV and another one between 6 and 7 keV. A hump near 5 keV is an artifact caused by a discontinuity in the pulse-height vs. energy relation of the GSPC at the Xe-L absorption edge (Koyama et al. 1984). The hump between 6 and 7 keV

Space Science Reviews **40** (1985) 317–338. 0038–6308/85.15.

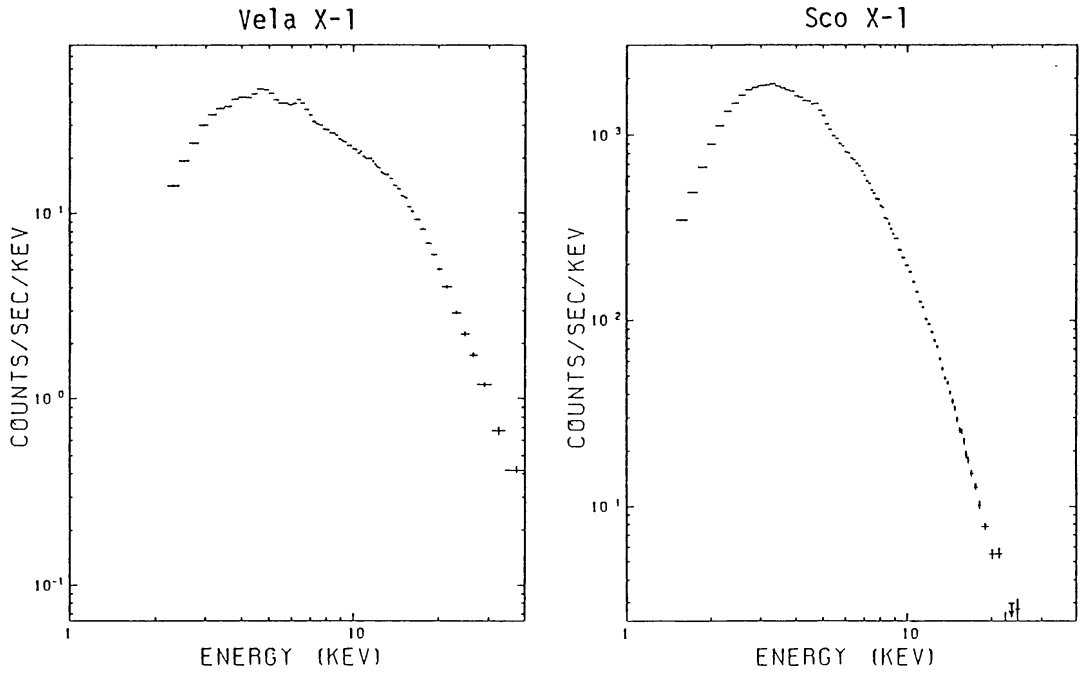

Fig.1 Pulse-height spectra of Vela X-1 and Sco X-1.

is considered to be the K-emission line of iron. The essential difference in the iron line emission from the two classes of sources is the line energy. The line center energy of the iron line from X-ray pulsars is estimated to be about 6.4 keV, whereas that from low-mass binary sources is about 6.7 keV. In this paper, we will first present the observational results of the iron emission line and will discuss likely candidates for the line emitting regions in the two different systems. The continuum spectra of the two classes are also different, as seen from Fig.1. The spectra of X-ray pulsars are generally expressed with a power-law spectrum, whereas low-mass binary sources reveal softer spectra approximated by a bremsstrahlung with kT $\simeq$ 5 keV. These distinctions are considered to be due to the fact that young neutron stars in X-ray pulsars possess a strong magnetic field, whereas the magnetic field is much smaller for old neutron stars in low-mass binary sources. From this point of view, the nature of the continuum emission from low-mass binary X-ray sources will be discussed, secondly. Finally, we will briefly comment on the X-ray spectra of the black hole candidate sources by comparing them with those of low-mass binary sources.

2. IRON LINE EMISSIONS FROM BINARY X-RAY SOURCES

2.1 X-Ray Pulsars

Tenma has observed 11 X-ray pulsars so far (see Table 1, and Nagase et al. for the details of pulse periods). All except three of the sources are consistent with emission of an iron line at 6.4 keV. Presence of a line from 4U1907+09 is marginal due to a contamination from a neighbouring SNR (Makishima, Koyama et al. 1984). Two peculiar pulsars;

Table 1. X-ray pulsars observed by Tenma

Source Name	Date of Observation	Pulse Period(sec)	Line Energy(keV)
Vela X-1	1983. 3. 3-18 1984. 3.23-26	282.9	6.43±0.05
Cen X-3	1983. 4. 4- 6 1984. 4.17-18	4.83	6.42±0.06
4U1626-67	1983. 5. 2- 6	7.67	———
Her X-1	1983. 5.21-30	1.24	6.41±0.05
4U1538-52	1983. 6.28-7. 6	529.8	6.4±0.3
4U1700-37	1983. 7.18-22	67.	6.47±0.07
OAO1657-415	1983. 7.18-23	37.9	6.48±0.07
4U1907+09	1983. 8.29-9. 7	437.5	———
A0535+26	1983.10.24-27	103.3	6.6±0.2
V0332+53	1983.11.14-12. 1 1983.12.31-84.1.5	4.37	———
GX301-2	1984. 4.23-27	701.5	6.49±0.06

4U1626-67 and V0332+53 reveal no significant emission line and their upper limits are estimated to be about 40 eV for both (Kii, Nagase et al. 1984, Makishima et al. 1984). The properties of the iron line emission were studied in detail for two pulsars: Vela X-1 and GX301-2. The results from GX301-2 will be presented seperately (Makino et al. 1984), and we will discuss the origin of the line emission by using Vela X-1 results (Ohashi et al. 1984).

The energy and the width of the iron line are determined to be 6.43 ± 0.05 keV and less than 0.5 keV (FWHM), respectively. K-line energy of iron is plotted in Fig.2 as a function of the ionization state (Morita and Fujita, 1983). As seen from this figure, the ionization state of line-emitting iron is between FeI and FeXIX.

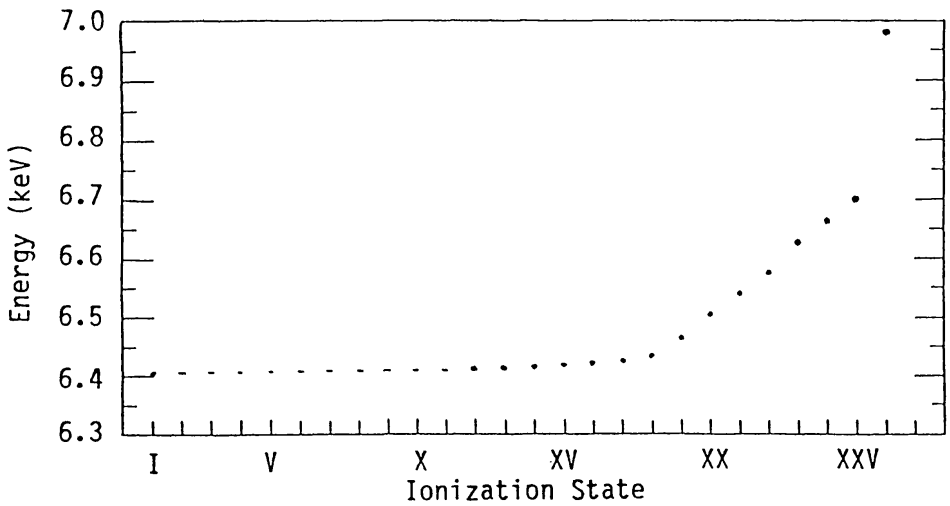

Fig.2 K-line energy vs. ionization state of iron.

Fig.3 shows the iron line intensity plotted for Vela X-1 against its continuum intensity in 7.1 - 30 keV. For the continuum intensity, absorption due to intervening gas and the efficiency of the instrument are corrected for. Although the fluctuations are quite large, a proportionality is seen between the iron line and the continuum intensities. This relation and the observed energy of the line indicate that the iron line from Vela X-1, (and probably every X-ray pulsar), is produced through the fluorescence of continuum X-rays by cold material.

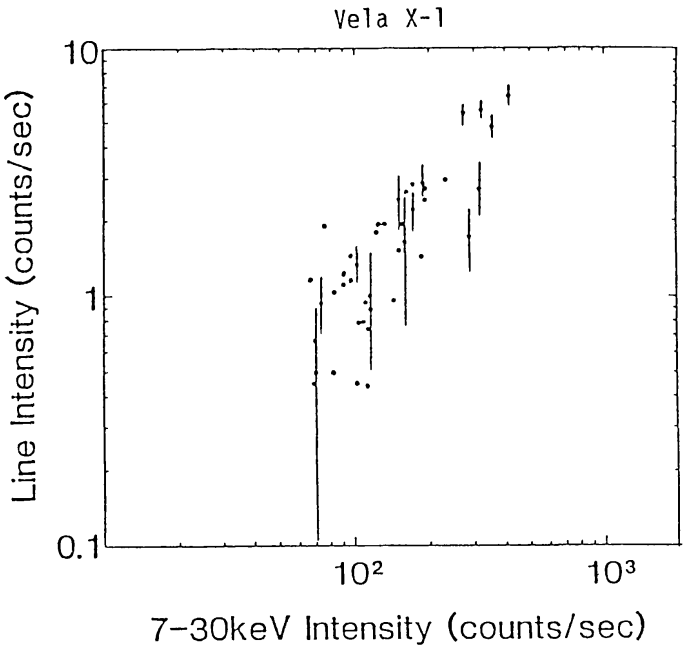

Fig.3 Line intensity vs. continuum intensity above 7.1 keV.

We performed a Monte Carlo simulation of the fluoresence iron line emission from neutral matter in a sphere surrounding an X-ray source as a function of the thickness of the matter N_H. Cosmic abundance of elements are assumed. Corresponding to an incident spectrum, dI/dE, three components emergent from the sphere were calculated:

(1) fluorescent iron line with its intensity, I_{Fe},

(2) directly observed continuum component, $(dI/dE)\exp(-\sigma N_H)$, where σ is the cross section of electron scattering + photoelectric absorption, and

(3) scattered component, dI'/dE.

Fig.4 shows results of the calculation. A power law spectrum with an index of 1.1 was assumed for the incident spectrum. Three solid lines, I, II and III, indicate, respectively, the equivalent widths of the fluorescent iron line estimated under three diferrent definitions as follows.

$$\begin{aligned} &\text{I.} \quad \text{E.W.} = I_{Fe} \,/\, (dI/dE)_{E=6.4\ \text{keV}} \cdot \\ &\text{II.} \quad \text{E.W.} = I_{Fe} \,/\, ((dI/dE)\exp(-\sigma N_H) + dI'/dE\ )_{E=6.4\ \text{keV}} \cdot \\ &\text{III.} \quad \text{E.W.} = I_{Fe} \,/\, (dI'/dE)_{E=6.4\ \text{keV}} \cdot \end{aligned} \tag{1}$$

The line I represents the fluorescence efficiency for the incident X-rays. The efficiency first increases with the thickness N_H of the gas. When N_H becomes larger than 5×10^{23} cm^{-2}, the efficiency starts to decrease. This is due to the absorption of the line photons within the gas. Hence, the efficiency has a maximum value around $N_H \simeq 5 \times 10^{23}$ cm^{-2}. This maximum value depends on the geometrical shape of the surrounding gas. If uniform matter in the sphere is confined into a thin shell, for example, the shell has a lower maximum value than that of the

sphere, as indicated with a dotted line in Fig.4. Furthermore, the fluorescence efficiency will be smaller, as the reprocessor subtends a smaller solid angle viewed from the central X-ray emitter. If the X-ray illuminated matter is outside the line of sight from the X-ray emitter to us, the incident spectrum can be directly observed. Then, the lower limit of the solid angle can approximately be obtained by comparing the observed equivalent width to the maximum value expected from the spherically surrounding matter.

On the other hand, if the matter is located between the X-ray emitter and an observer, the observed continuum spectrum suffers from absorption by the matter. In that case, the observed equivalent width should be compared to line II in Fig.4, where the equivalent width monotonously increases in proportion to the column density of the matter. Line III corresponds to the case when the central X-ray emitter is totally hidden by some thick material and only scattered emission from the ambient matter is observed.

GX301-2 is considered to correspond to the case II, which is discussed seperately (Makino et al. 1984). Whereas, case I is applied to Vela X-1 as discussed below. Further, a fact that the equivalent width as large as 1 keV is observed from Vela X-1 during its eclipse (Ohashi et al. 1984, Sato, Nagase et al. 1984) is consistent with case III.

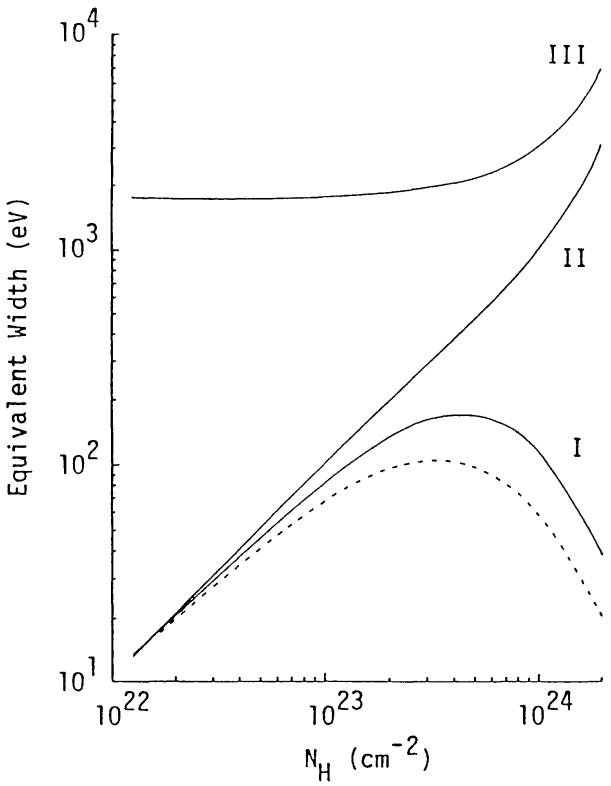

Fig.4 Expected equivalent width of fluorescent iron 6.4 keV line.

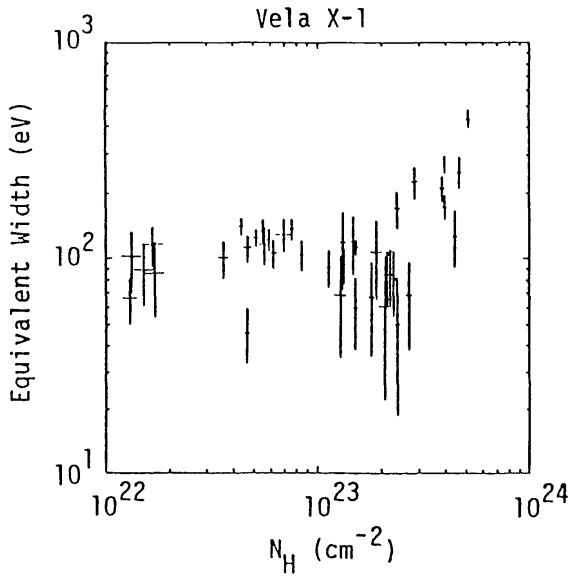

Fig.5 Observed equivalent width vs. column density relation.

The equivalent width of the 6.4 keV line and the column density of intervening gas N_H are evaluated through a spectral fit to each Vela X-1 spectrum for a 10 - 30 min. interval and their values are plotted in Fig.5. Although N_H values range widely from 2×10^{22} to 5×10^{23} cm^{-2}, the observed equivalent width of the iron line is mostly 100 to 150 eV, independent of N_H. Even for $N_H \simeq$

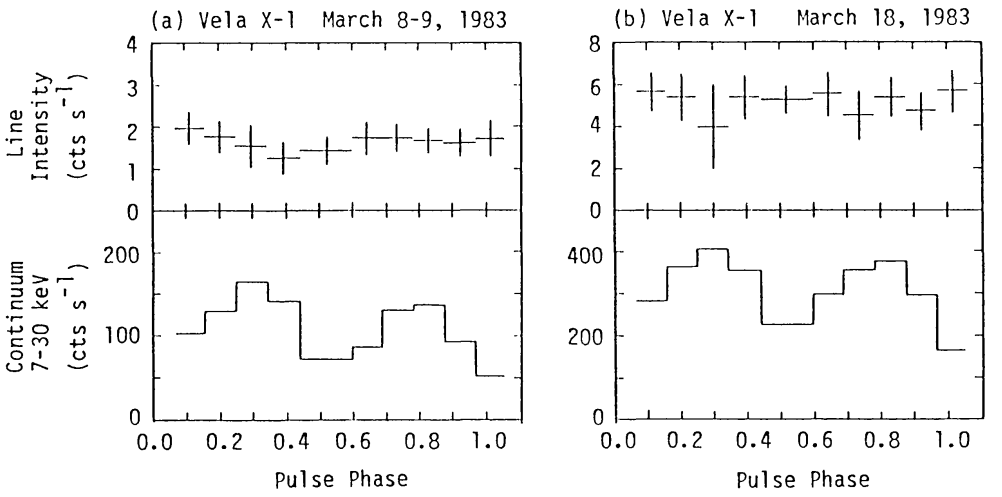

Fig.6 Pulse-phase dependency of the iron line intensity.

10^{22} cm^{-2}, the observed equivalent widths are as large as 100 to 150 eV. Hence, a thick matter with $N_H > 10^{23}$ cm^{-2} must be present out of the line of sight.

On the other hand, the equivalent width of the iron line at 100 - 150 eV is almost equal to the maximum value for a gas shell, which indicates the covering factor of the reprocessing matter to the X-ray emitter is almost 100%. The 100% covering is also suggested from observed lack of pulse-modulation of the line intensity. As shown in Figs.6(a) and (b), the line intensity is consistent with a constant value over the whole pulse phase, though continuum intensity levels vary by a factor of 3 for these two cases. The absence of the pulse modulation can be easily explained by a reprocessor spherically surrounding the neutron star.

Now, we need to understand two necessary conditions that contradict each other. The reprocessor with $N_H > 10^{23}$ cm^{-2} must receive nearly all of the X-ray emission, but must be outside the line of sight from the neutron star to us. This will be realized only when most of the X-ray emission from the neutron star is confined in a pencil beam. If the intense X-ray beam is incident on the reprocessor, a reprocessor which subtends a significantly smaller solid angle may suffice to produce the observed iron line. Furthermore, the absence of the pulse modulation of the iron line would suggest that the relative orientation of the reprocessor to the X-ray beam does not change with the rotation of the neutron star. The absence of the pulse modulation of the line intensity can be explained by the isotropic emission of the fluorescent iron line, which will be expected when the matter is optically thin to the line photons, i.e., when $N_H \lesssim 2 - 3 \times 10^{23}$ cm^{-2}.

Column density of stellar wind matter can be as thick as 10^{23} cm^{-2}. Figure 7 shows the variation of the iron line intensity of Vela X-1 through the eclipse. The iron line intensity during eclipse is about a tenth of that outside the eclipse. The presence of the iron line intensity during the eclipse indicates that a certain fraction of the iron line comes from the stellar wind matter. However, the time scale of the line intensity variation at the ingress and egress of the eclipse sets

the upper limit for the main line emitting region, which is estimated to be about 10^{11} cm at largest. The typical dimension of the stellar wind matter is of the order of 10^{12} cm, and is too large compared with the above upper limit. Hence, a large fraction of the iron line probably comes from the region near the neutron star.

A more likely candidate for the line emitter is accreted matter trapped in the Alfven shell of the neutron star. Accreted matter inside the Alfven shell tends to gather near the polar axis of the magnetic field of the neutron star, and to corotate with the neutron star. Hence, such matter will satisfy the geometrical condition for the line emitter as discussed before. Thus, the main questions are the matter has the column density as thick as a few 10^{23} cm^{-2} and why iron is less ionized than XX under the intense X-ray illumination.

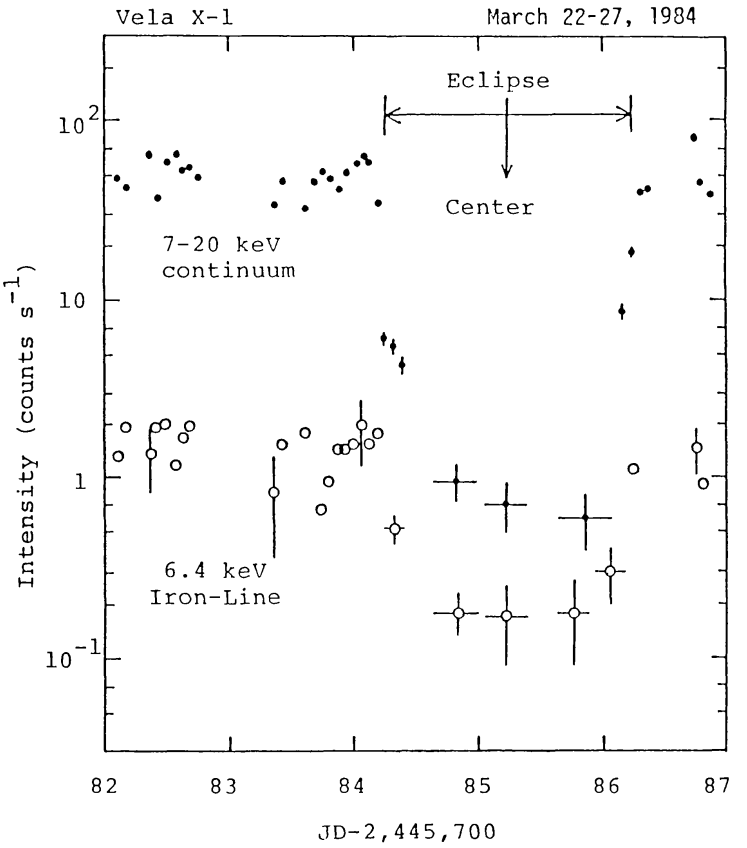

Fig.7 Intensity variation of Vela X-1 through the eclipse.

The column density N_H of the matter accumulated on the Alfven shell is approximately calculated in terms of the accumulated matter ΔM and the surface area S, as $N_H \simeq \Delta M / m_H S$, where m_H is the hydrogen mass. Here, the amount of the accumulated matter ΔM is estimated as a function of the accretion rate $\dot{M}$ and the staying time Δt on the shell at the distance r_A from the nautron star, as $\Delta M \simeq \dot{M} \Delta t$. The surface area S is roughly expressed as $S \simeq \Omega r_A^2$, where Ω is the solid angle of the matter as viewed from the neutron star. Thus, N_H is approximately written as

$$N_H \simeq \dot{M}\alpha/(m_H\Omega(2GMr_A)^{1/2})$$
$$= 2.9 \times 10^{22}(4\pi/\Omega)\alpha(\dot{M}/10^{17})(M/M_\odot)^{-1/2}(r_A/10^8)^{-1/2} \text{ cm}^{-2}, \quad (2)$$

where $\alpha \equiv \Delta t / (r_A^3/2GM)^{1/2}$; ratio of the staying time to the free-fall time. Hence, under a reasonable assumption that $r_A \simeq 10^8$ cm, $\alpha \gtrsim 1$ and $\dot{M} \simeq 10^{16\text{-}17}$ g sec^{-1}, the reprocessor with the thickness of the order of 10^{23} cm^{-2} can be obtained at the polar region with $\Omega/4\pi \lesssim 0.1$.

The next question is about the ionization state of iron on the Alfven shell. The ionization degree of matter illuminated by intense X-rays is determined in terms of a parameter $\xi \equiv L/nr^2$, where L is illuminating X-ray luminosity, n the number density of the ambient gas and r

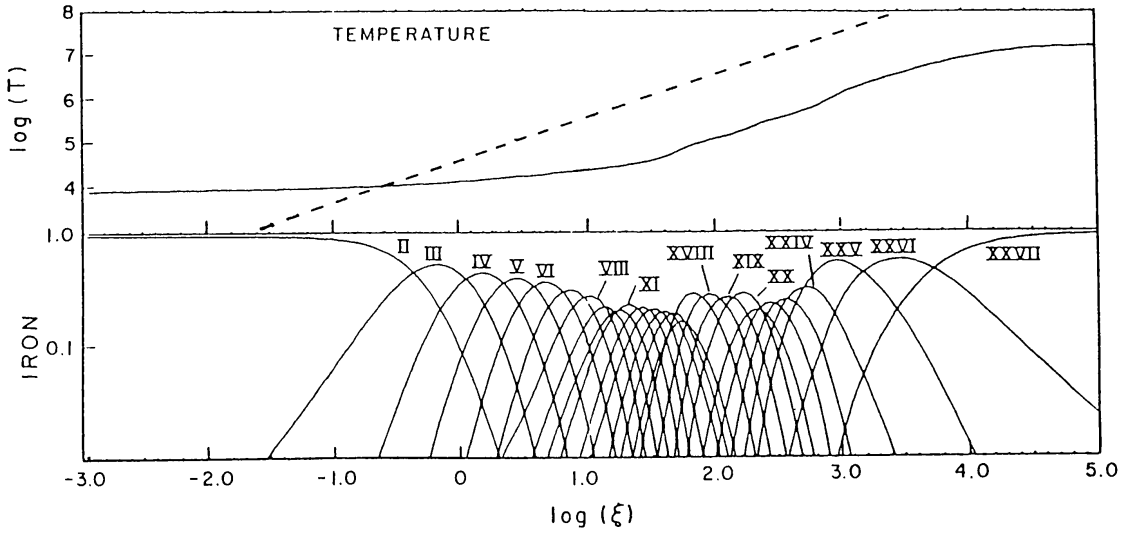

Fig.8 ξ - T relation expected on the Alfven shell.

its distance from the X-ray source (Tarter et al. 1969). The number density of the shell material is calculated from $n \simeq N_H/d$, where d is the geometrical thickness of the shell. The parameter d is roughly given through a hydrostatic equation on the Alfven shell as $d \simeq kTr_A^2/m_H GM$, and finally ξ is expressed as

$$\xi \simeq 2.8\ ((\Omega/4\pi)/0.1)\alpha^{-1}(R/10^6)(M/M_\odot)^{3/2}(r_A/10^8)^{1/2}(T/10^5)$$

$$\text{erg cm sec}^{-1}, \quad (3)$$

where $L = \dot{M}GM/R$ is assumed and R is the radius of the neutron star.

The relation of $\xi = 2.8\ (T/10^5)$ erg cm sec^{-1} is plotted with a dashed line in Fig.8. On the other hand, X-ray heating and radiative cooling balances on a solid line, which is calculated by Kallman and McCray (1982), together with the ionization degree of iron also shown in this figure. Although this equilibrium line represents one example among the many cases considered by Kallman and McCray (1982), the ξ - T relation of the thermal balance does not largely change case by case. Since the cross point of the two lines will be realized in the matter on the Alfven shell, we can see that iron atoms on th Alfven shell will stay in very low ionization state.

2.2 Low-Mass Binary Sources

Tenma observed more than ten low-mass binary sources. Most of their spectra reveal an emission line near 6.7 keV. However, since they are usually near the galactic plane, and with a fairly large field of view of a 3°(FWHM) circle, Tenma GSPCs always detect a diffuse 6.7 keV line simultaneously with the source component. Tenma discovered that a prominent iron line at 6.7 keV comes from near the galactic plane but not associated with known sources (Koyama 1984). Hence, properties of the emission line from the low-mass binary source has been studied in detail only for two bright sources, Sco X-1 and 4U1608-52 (Suzuki et al. 1984).

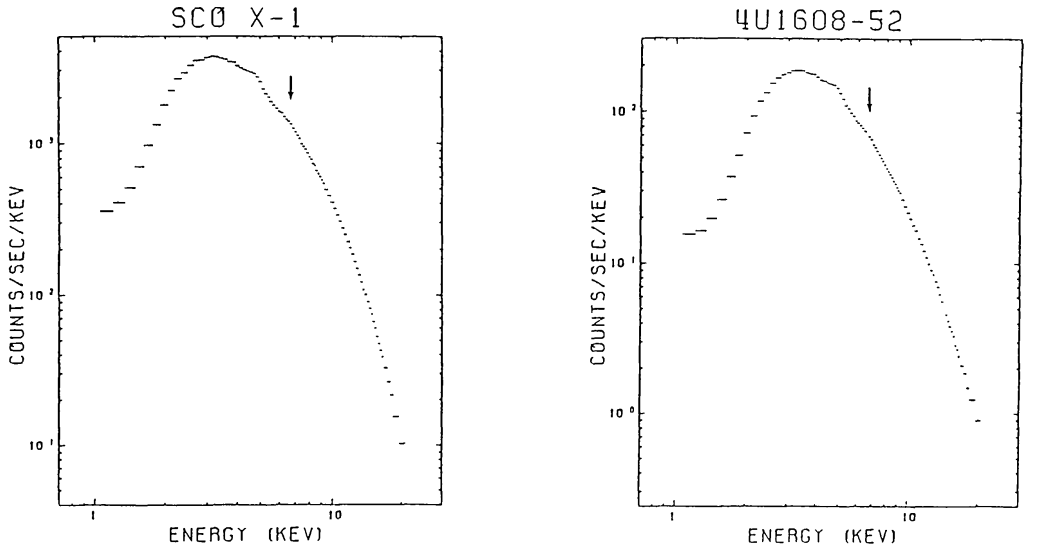

Fig.9 Pulse-height spectra of Sco X-1 and 4U1608-52.

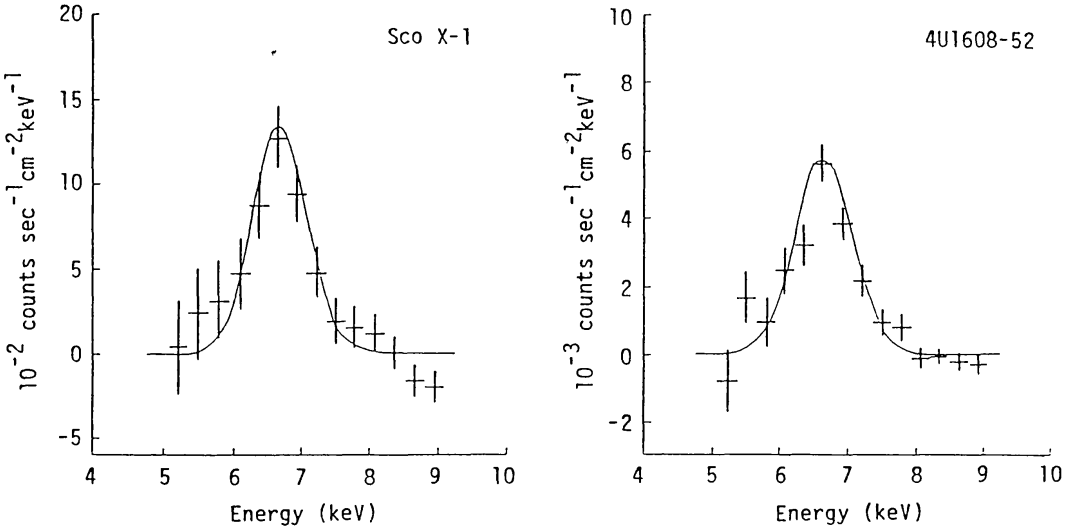

Fig.10 Emission line spectra of Sco X-1 and 4U1608-52.

4U1608-52 was in the bright phase during April to July, 1983.

Figures 9 and 10 show pulse-height spectra obtained from the two low-mass binary sources, and their emission line spectra after subtracting the best fit continuum spectra, respectively. For the continuum model, we employed two components model which will be dicussed later. Solid lines in Fig.10 represent best fit curves, where three parameters for the line: the line center energy, the line intensity and the FWHM line width, were adjusted to minimize the χ^2 value. Acceptable ranges for the three parameters are indicated in Fig.11. The intrinsic line width and the equivalent width are closely correlated with each other. This is due to the uncertainty of the continuum level. If one underestimated the local continuum, the line intensity and the line width are overestimated. Thus, the acceptable range for the equivalent width is fairly large, from 30 to 100 eV. Whereas, the line center energy is not so strongly correlated with the other, and is determined to be 6.67 ±

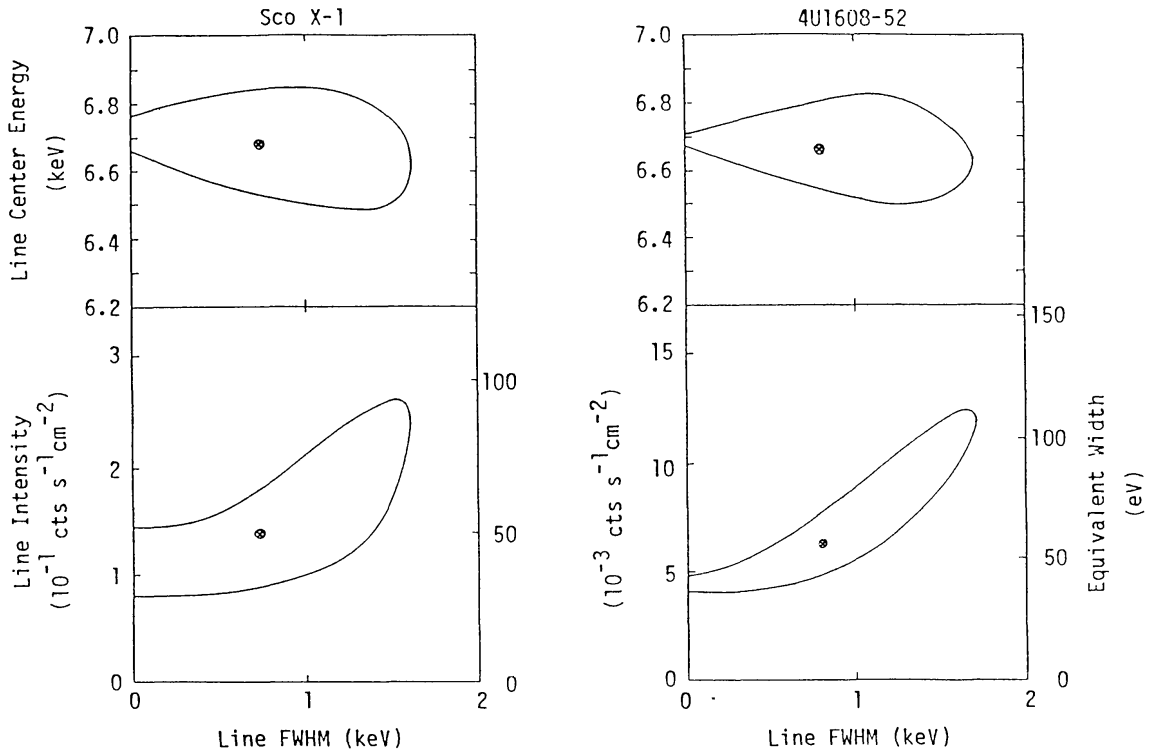

Fig.11 Uncertainty ranges of three parameters for the line.

0.17 keV.

The uncertainty range of observed line center energy includes the K-line of FeXX-XXV (see Fig.2). However, since the helium-like iron (FeXXV) has largest efficiency for K-line emission, the observed emission line is considered most probably to be the K-line from helium-like iron.

Two possibilities can be considered for the origin of the 6.7 keV line. One is the thermal emission form a thin hot plasma, where iron atoms are collisonally excited. The other is a fluorescent emission from a plasma illuminated by the continuum X-rays, where iron atoms are subject to photo-ionization.

The equivalent widths of iron lines expected from a thin hot plasma are plotted as a function of the temperature in Fig.12 (Raymond and Smith 1977). The equivalent width of the 6.7 keV FeXXV line can go as high as 1 keV in the temperature range (2-4) x 10^7 K. Therefore, the presence of a thin hot plasma in this temperature range would explain the observed equivalent width of several tens of eV, if the

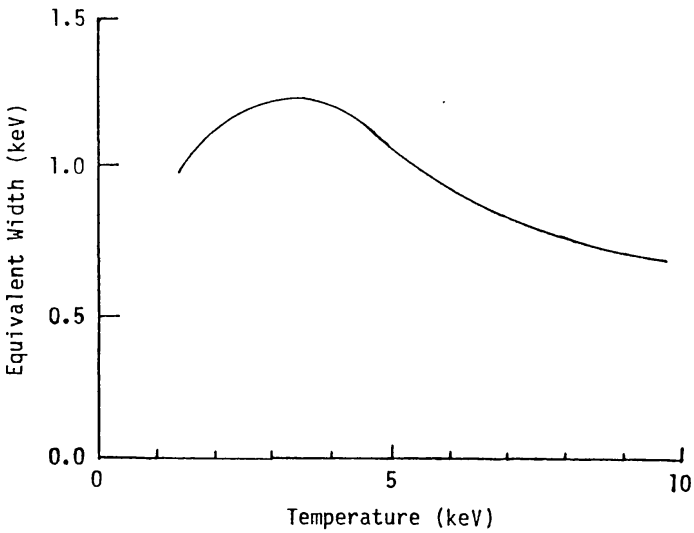

Fig.12 Equivalent width of 6.7 keV line from a thin hot plasma.

thermal emission from this plasma amounts to one tenth of the total luminosity. However, a difficult problem is what is the energy source of the thermal emission? If gravitational energy release is to account for the luminosity of the thin hot plasma, the plasma should be located at a distance of the order of 10^7 cm from the neutron star (one tenth of the gravitational potential at the neutron star surface). On the other hand, an optically thin plasma, if placed at such a close distance, would become much higher in temperature than 10^8 K. Thus, stationary presence of a thin plasma of several 10^7 K seems hardly plausible.

The fluorescence process is more likely to account for the observed iron K-line. The fluorescence process for helium-like ions, however, is different from that for neutral ions. In the case of neutral iron, a fluorescent line is emitted when an L-electron falls to the ground-level after a photoionization of a K-electron. The probability of the K-line emission after a K-photoionization is about 34%, and the remaining probability is for the Auger process. In the case of helium-like iron, on the other hand, a K-fluorescent line is emitted when a free electron is recombined to a level higher than the ground level after a K-photoionization, and the electron cascades to the ground level. The probability of the line emission after a K-photoionization is approximately given by the probability of the recombination to the levels higher than the ground level, which is estimated to be about 82% in the case of FeXXV 6.7 keV line (Tucker 1977, Basko 1980). The effect of the self-absorption of the iron line is also different in the two cases. When iron atoms are ionized up to be helium-like by X-ray illumination, other abundant and lighter elements are almost fully ionized and hence the effect of self absorption of 6.7 keV line is very small compared with that of 6.4 keV line.

After the above considerations were taken into account, a Monte Calro simulation was performed for the fluorescence line emission from helium-like iron, as similar to the case of 6.4 keV line. Helium-like ions of iron are most abundant when $\xi \simeq 10^3$ erg cm sec^{-1} (Kallman and McCray, 1982). Then, hydrogen-like silicon, sulpher, argon and calcium mainly contribute to the absorption of the 6.7 keV line. After the calculations of the ionization degree by Kallman and McCray (1982), the fraction of hydrogen-like ions are assumed to be 0.2, 0.3, 0.5 and 1.0 for the four elements with cosmical abundances, respectively. For an incident spectrum, we employed a Planckian distribution with kT = 2 keV, which well reproduced the continuum spectrum above K edge energy as shown later. As seen from the results of the simulation in Fig.13 (for the definitions of lines I-III, see Eq.(1)), the equivalent width of

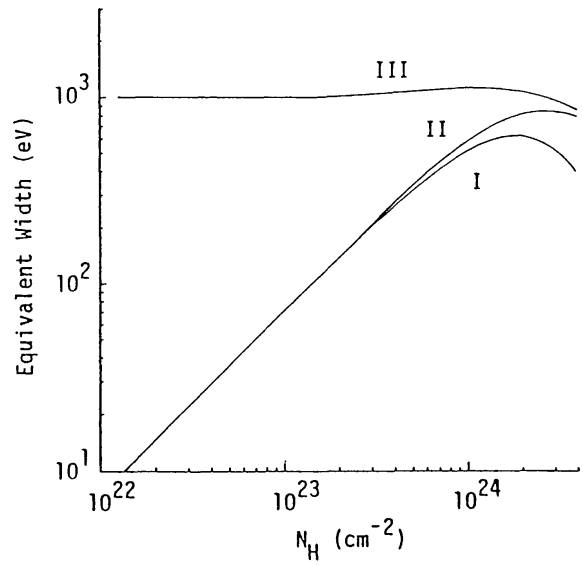

Fig.13 Expected equivalent width of 6.7 keV line from a sphere.

the 6.7 keV line is expected to be as high as 600-700 eV from a spherical gas with the thickness of $N_H \simeq 10^{24}$ cm^{-2}, surrounding the X-ray emitter. Hence, the observed equivalent width of several tens eV is obtainable, if the X-ray illuminated gas subtends a solid angle of about 1 sr. as viewed from the central X-ray sources.

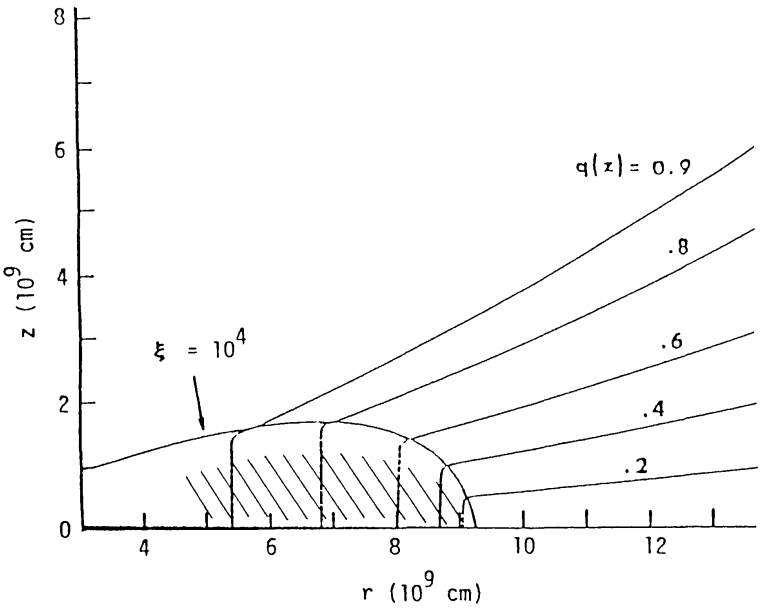

Fig.14 Schematic cross section of outer accretion disk (Hoshi 1984).

The accretion disk will extend as far as 10^{10-11} cm from the neutron star in the low mass binary sources. Since the energy flux of X-rays incident on the disk surface is large compared to the gravitational energy release of the disk material. Hence, the outer disk will be optically thin and geometrically thick (Hayakawa 1981, Hoshi 1984). Figure 14 shows the schematic cross section of the outer disk calculated by Hoshi(1984), taking full account of the effect of the X-ray illumination. The locus of $\xi = 10^4$ erg cm sec^{-1} is plotted as well as the loci of the constant fraction of the disk matter q(z), in this figure. When ξ is larger than 10^4 erg cm sec^{-1}, the plasma temperature tends to be the typical energy of illuminating X-rays (Hatchett et al. 1976). This condition is satisfied in the outer disk at $r \gtrsim 10^{10}$ cm. However, as r decreases from 10^{11} cm, the thermal energy with temperature of about 10^7 K become gradually smaller relative to the gravitational potential energy and the height of the disk shrinks. Hence, density becomes higher, and ξ cannot be so large as 10^4 erg cm sec^{-1} at $r \lesssim 10^{10}$ cm. Once ξ decreases below 10^4 erg cm sec^{-1}, the plasma temperature cannot be maintained at the X-ray energy so that the height of the disk shrinks further and further through radiative cooling. Finally, an optically thick disk will be realized inside the 10^{10} cm distance.

Helium-like iron is most abundant when $\xi \simeq 10^3$ erg cm sec^{-1} and $T \simeq 10^6$ K (Kallman and McCray, 1982); this region is schematically indicated with hatching in Fig.14. The solid angle of the disk viewed from the neutron star is roughly given, in terms of the half-thickness of the disk, d, by $4\pi d/r$. Hydrostatic equilibrium in the direction perpendicular to the equatorial plane of the disk determines the thickness of the disk as $(d/r) \simeq (rkT/m_H GM)^{1/2}$. Hence, the solid angle of the region where $r = 10^{10}$ cm and $T = 10^6$ K is estimated to be about 1 steradian. On the other hand, the equation $\xi \equiv L/nr^2 = 10^3$ erg cm sec^{-1} yields $N_H \simeq nr = 10^{24}$ cm^{-2} in case that $L = 10^{37}$ erg sec^{-1} and $r = 10^{10}$ cm. These values of the solid angle and the column density of this $\xi \simeq 10^3$ region well satisfy the necessary condition for the observed equivalent width

as discussed above.

2.3 A Peculiar Source: Cyg X-3

Tenma observed Cyg X-3 in Sept. 1983 and Sept. 1984. The pulse height spectra averaged over each of the two observational periods are plotted in Fig.15, and both reveal an prominent emission line at 6.7 keV (Kitamoto et al. 1984). The iron line intensities and the equivalent widths in the two periods are ploted in Fig.16 as a function of 4.8 hour modulation phase. Note that the iron line intensity is almost constant against the large 4.8 hour modulation of the equivalent width.

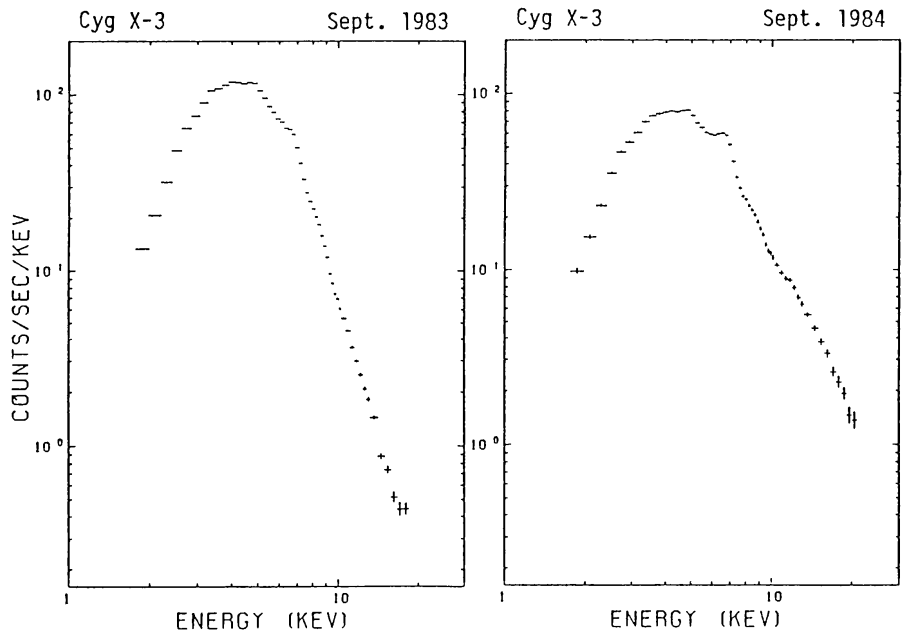

Fig.15 Pulse-height spectra of Cyg X-3.

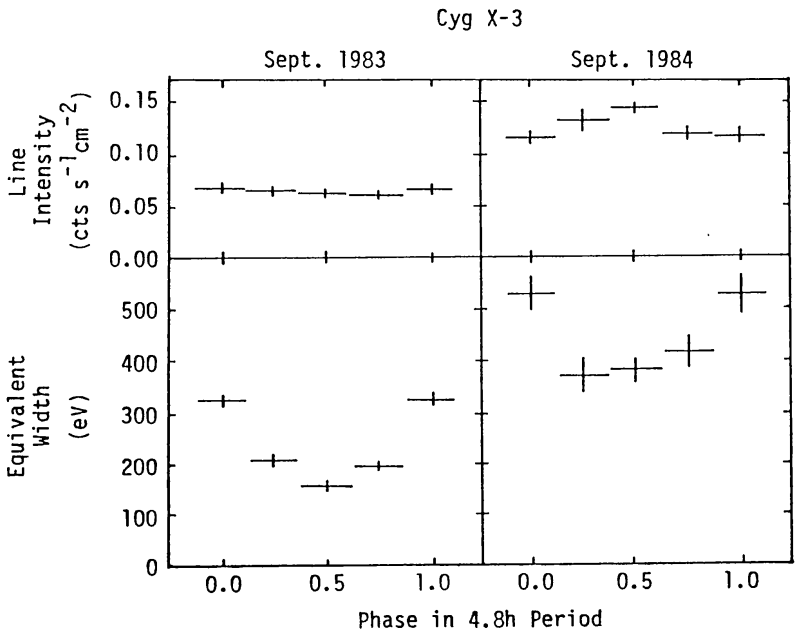

Fig.16 4.8 hour modulation of line intensity and Equiv. width.

The equivalent width of the 6.7 keV line is as large as 200 to 500 eV. Although existence of a thin hot plasma is possible to account for this large equivalent width, a severe difficulty is the energy source of the thermal emission, similar to the case of low-mass binary sources discussed before. The fluorescence process is a more likely origin of the line emission in this case also. This is supported by a proportionality between the line and the 9-10 keV intensities averaged over 4.8 hour period, as shown in Fig.17. However, an equivalent width as large as 200 to 500 eV indicates the presence of a highly ionized matter which subtends a solid angle as large as or larger than 2π sr. viewed from the central X-ray source. It seems difficult to have the X-ray illuminated outer accretion disk emit such an intence emission line, in this case. If the 4.8 hour modulation reflects the orbital motion of some scattering matter around the compact X-ray source (Pringle 1974, Milgrom 1976), the lack of strong 4.8 hour modulation of the iron line suggests that the line emitting matter almost wholly surrounds the compact object plus scattering matter system.

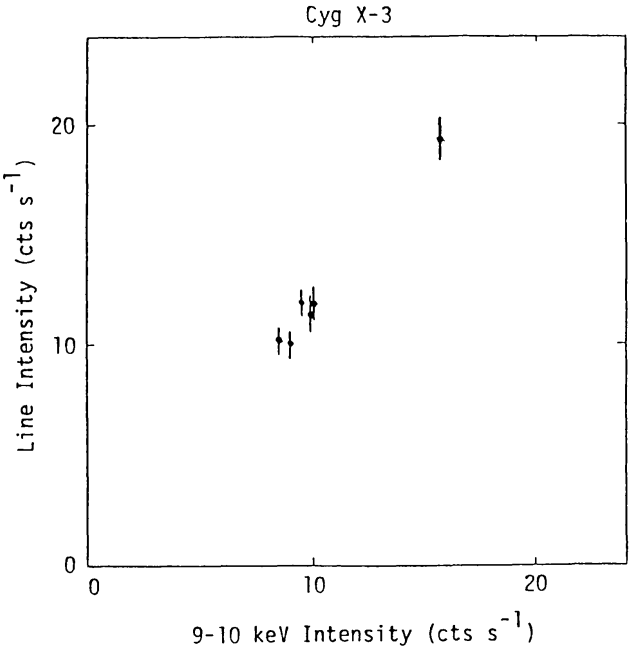

Fig.17 Line intensity vs. 9-10 keV intensity relation of Cyg X-3.

3. CONTINUUM SPECTRA OF LOW-MASS BINARY SOURCES

3.1 Two Emission Regions near A Weakly Magnetized Neutron Star

Observed spectra of low-mass binary sources are softer than those of X-ray pulsars. The soft spectra of low-mass binary sources are considered due to that the magnetic field of the neutron star is not so strong as that of X-ray pulsars. If the magnetic field of the neutron star is too weak to influence the accretion flow, the accretion disk will extend to the neutron star surface.

In the standard accretion disk model (Hoshi 1984, and references therin), the inner most region of the disk is optically thin and the optically thick disk rotates around it. In the accretion disk, the matter circulating along the Keplerian orbit gradually falls inward, and the gravitational energy released will be evenly converted to thermal and rotational energies. If the accretion disk is optically thick, the thermal energy will be sufficiently radiated away from the disk. However, the emissivity is very low in the inner optically thin region and the most of the thermal energy will be carried over to the neutron star surface. This thermal energy in the inner region and the rotational

energy will be released when the disk matter lands on the neutron star surface. Therefore two seperate emission regions are expected; the surface of the optically thick accretion disk and the neutron star surface.

The flux from the optically thick accretion disk, $f_d(E)$, is given by integrating the local blackbody spectrum;

$$f_d(E) = (\cos\theta / D^2)\int_{r_{in}}^{r_{out}} 2\pi r\ B(E,T)\ dr, \tag{4}$$

where $B(E,T)$ is the Planckian distribution with a tenperature T, θ is the inclination angle of the line of sight to the accretion disk, D is the distance of the source, and r_{in} and r_{out} are the inner and outer boundaries of the optically thick disk. Since T is proportional to $r^{-3/4}$ on the surface of the optically thick disk, the above equation is rewritten as;

$$f_d(E) = (8\pi\cos\theta / 3D^2)\ r_{in}^2\int_{T_{out}}^{T_{in}} (T/T_{in})^{-11/3}\ B(E,T)\,dT/T_{in}, \tag{5}$$

where T_{in} and T_{out} are the temperatures at the inner and outer boundaries, respectively. Since T_{out} is considered to be negligibly small compared with T_{in}, the above spectrum is represented by only two parameters; r_{in} and T_{in} in the energy range interested here.

On the other hand, the flux from the neutron star surface is written as

$$f_b(E) = (S'/ D^2)\ B(E,T_b), \tag{6}$$

where S' is the projected area of the emission region.

3.2 Two Components in Observed Spectra

Tenma observed four low-mass binary sources as bright as 10^{37-38} erg sec^{-1}: Sco X-1, 4U1608-52, GX5-1 and GX349+2 (Mitsuda et al. 1984). All four sources showed intensity variations by a factor of two to three on a time scale of a few hours. We found that all the observed spectra can be explained by a sum of two components: a hard and a soft components, and the temporal variation is mainly due to the intensity variation of the hard component.

Figure 18 shows examples of the energy spectra of the four sources. These spectra can be decomposed into two spectral components (for the detail of the decomposition see Mitsuda et al. (1984)). A hard component is well represented by a blackbody spectrum with a temperature of about 2 keV. On the other hand, a soft component is well reproduced by a "multi-color" spectrum expected from an optically thick accretion disk.

The shapes of both components are consistent to be constant with time. The temperature of the blackbody spectrum from the neutron star surface, T_b, and the temperature at the inner edge of the optically

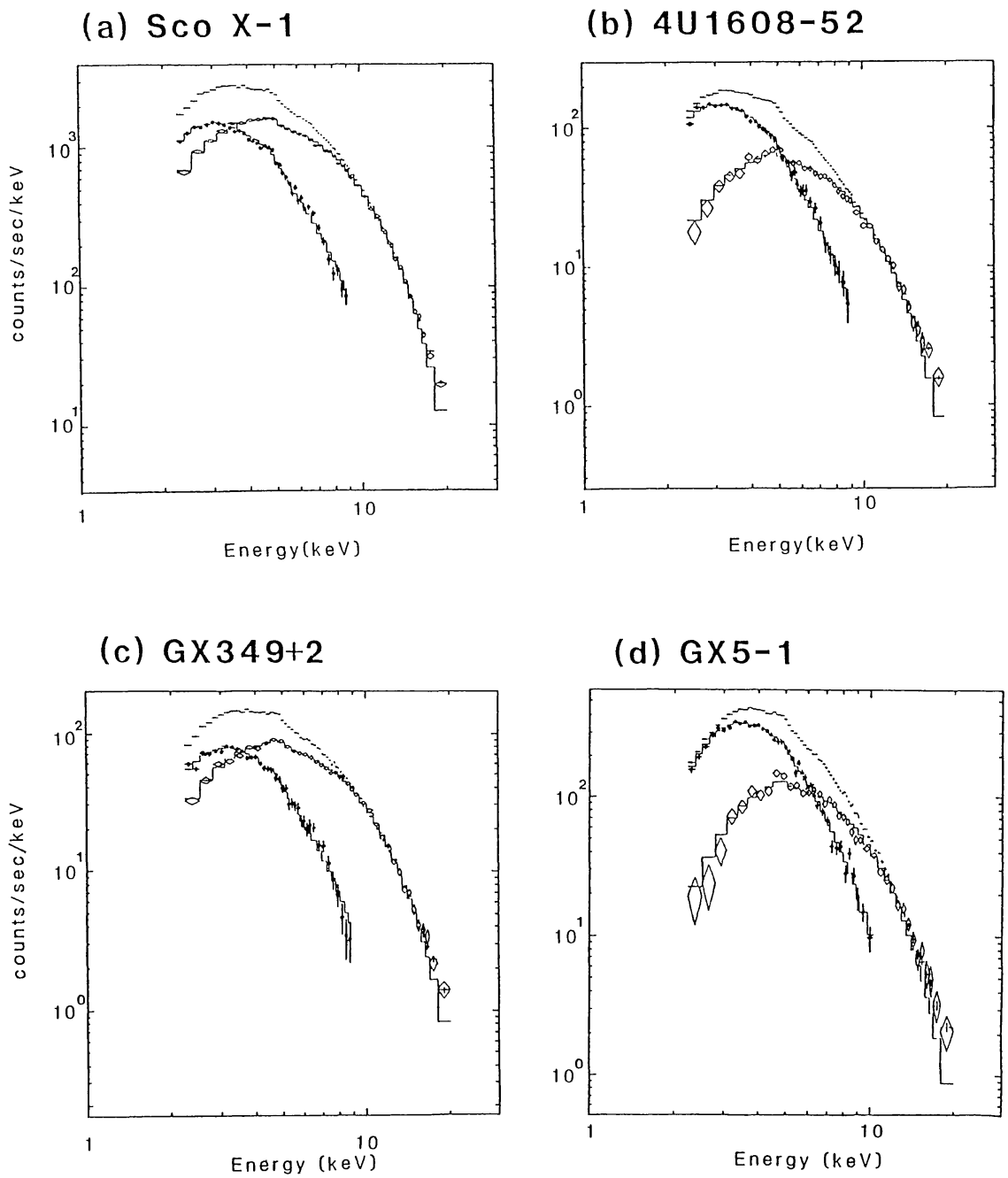

Fig.18 Pulse-height spectra of four bright low-mass binary sources. Crosses, diamonds and crosses with filled circles represent the observed spectra, decomposed hard and soft components, respectively. Solid lines are best fit curves for the two components.

thick accretion disk, T_{in} are summarized for the four sources in Table 2. It is striking that these temperatures are not only constant with time for each individual source but also about the same for different sources.

Figure 19 shows the intensities of the two components as functions of time. We clearly see that the soft component is quite stable, while the hard component is highly variable.

Table 2. Parameters of the spectra of the four sources

Source	kT_b(keV)	kT_{in}(keV)
Sco X-1	2.00±0.03	1.38±0.06
4U1608-52	2.11±0.03	1.30±0.06
GX349+2	2.12±0.03	1.44±0.08
GX5-1	1.97±0.05	1.36±0.06

Figure 19 also gives the two quantities (right hand scale), $R' \equiv (S'/\pi)^{1/2}$ and $r_{in}' \equiv r_{in}(\cos\theta)^{1/2}$, which are derived from the two components fittings of each observed spectrum. The distance D is fixed to be 10 kpc. The observed results always satisfy the relation $r_{in}' > R'$. This is consistent with the concept that the emitting area of the hard component is always smaller than that of the soft component.

In the case of 4U1608-52, Tenma detected X-ray bursts from this source. The radius of the neutron star can be obtained from the spectral analysis of the burst. It is genarally believed that each burst covers the entire surface of a neutron star. Figure 20 shows an example of X-ray bursts from 4U1608-52, where results of the blackbody fittings to time resolved X-ray burst spectra: energy flux, color temperature and

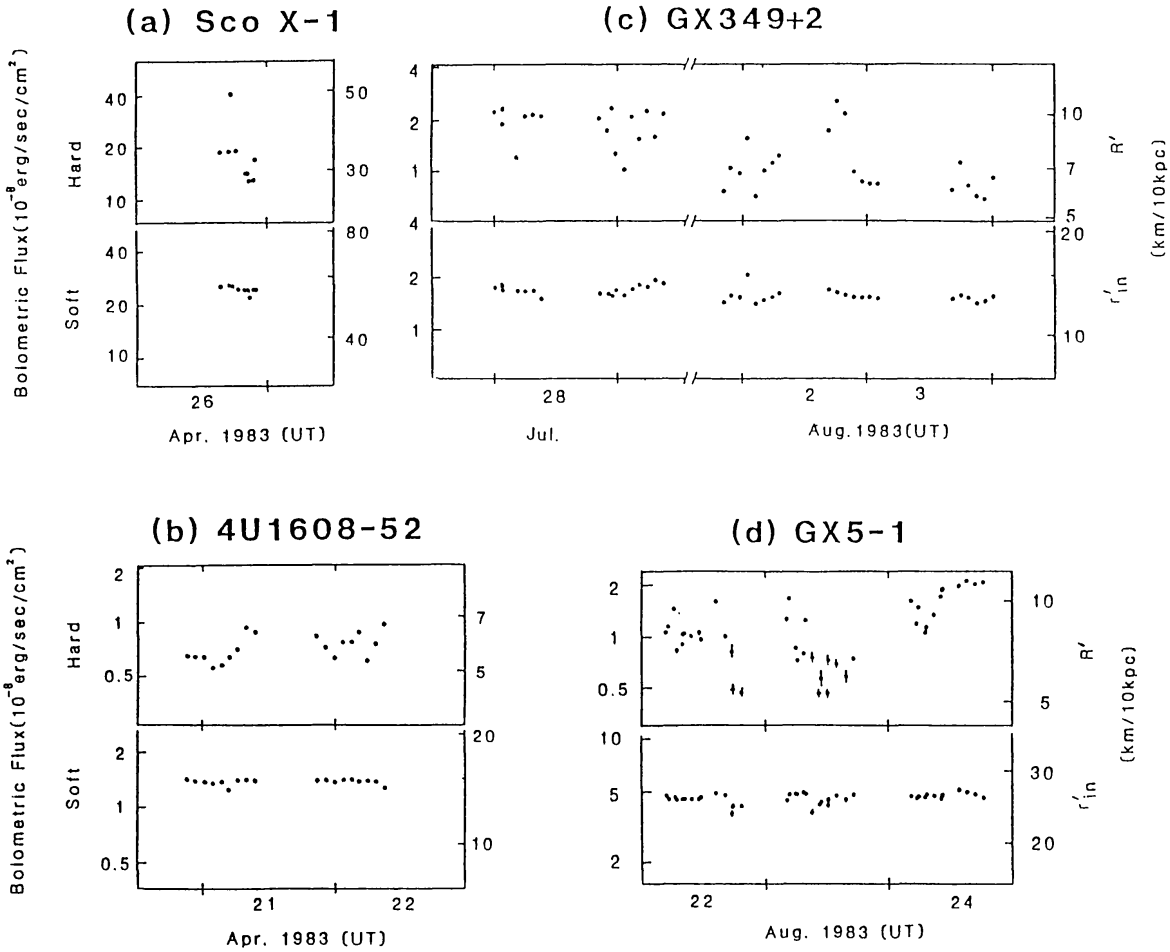

Fig.19 Intensity variations of the two spectral components.

apparent radius (R_a), are plotted as a function of time from the burst onset. By comparing this figure to Fig.19-(B), we can obtain the following inequality;

$$R' < R_a \simeq r_{in}' \leqq r_{in} . \quad (7)$$

While the inclination angle θ is unknown and the effect of the electron scattering on the apparent blackbody radius cannot be neglected (Inoue, Waki et al. 1984, and references therein), the above inequality is quite consistent with that the 2 keV blackbody component is from some small region on the neutron star surface while the soft component is from an optically thick accretion disk outside the neutron star.

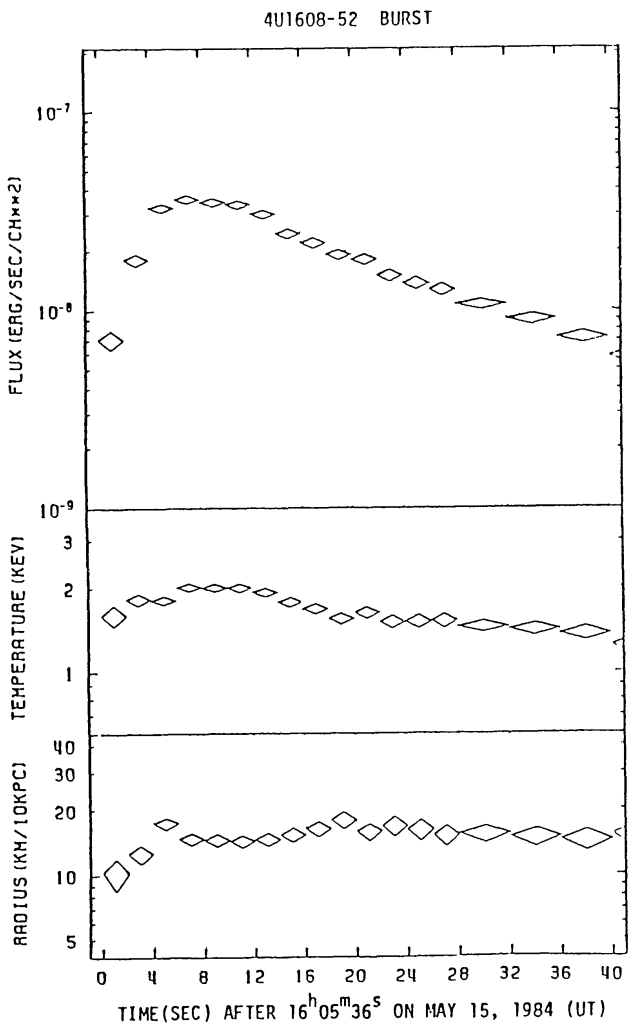

Fig.20 A X-ray burst from 4U1608-52.

3.3 Reservoir near Neutron Star ?

As regards the soft component, the derived accretion disk parameters T_{in} and r_{in}' are found to be remarkably constant in spite of large changes of the hard component. This fact would imply that the accretion flow itself down to r_{in} is kept fairly constant with time. Whereas, the flow inside r_{in} may be variable to cause large changes of the hard component. This suggests the presence of some instability in the flow and, at the same time, some reservoir of the accreted matter inside r_{in}.

The reservoir of the accreted matter will be helpful to explain some other observational facts in low-mass binary sources. One is the relation between type I X-ray burst activity and the persistent emission. In the canonical model for type I bursts, the integrated burst flux must be in proportion to the persistent flux integrated over the interval to the preceding burst. However, the burst activity occasionally independent of the persistent flux variation (Ohashi 1981). In particular, the presence of the reservoir seems inevitable for the interpretation of successive bursts with a short interval of about 10 minutes (Inoue, Koyama et al. 1984, and references therein). Another phenomenon indicating the existence of the reservoir is type II bursts from the rapid burster (Kunieda et al. 1984, and references therein). These topics of X-ray bursts will be seperately presented by Tanaka (1984).

3.4 Spectral Hardening with Decreasing Intensity $\lesssim 10^{36}$ erg sec^{-1}

The intensity of a soft transient source 4U1608-52 decreases by an order of magnitude from 1983 to 1984. In April to July, 1983, this source was as bright as 10^{37-38} erg sec^{-1}. Its spectrum was, always through the observational period, consistently composed of two component: a 2 keV blackbody and a "multi-color" accretion disk component, as discussed

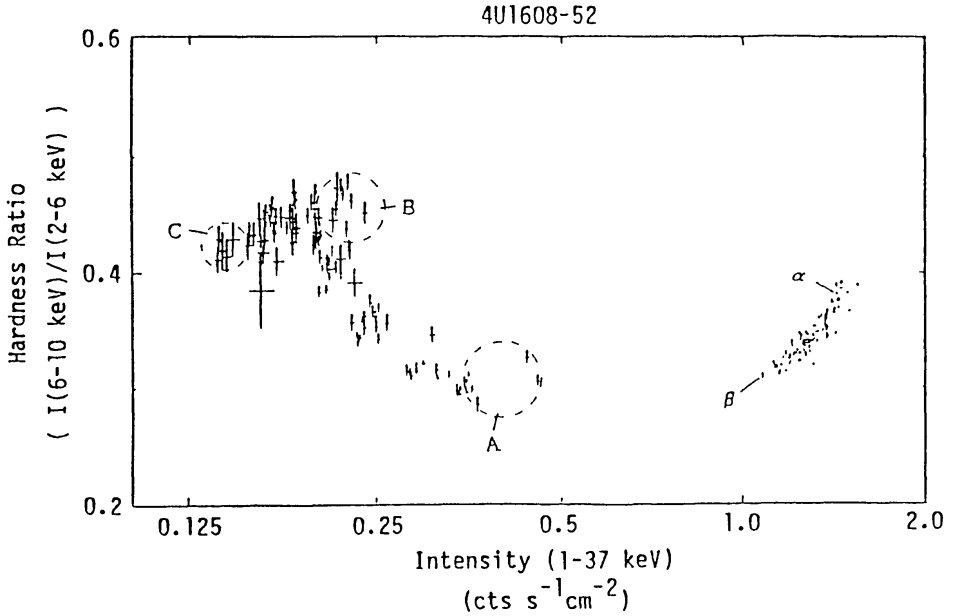

Fig.21 Hardness ratio vs. total intensity of 4U1608-52.

above. In May to June, 1984, however, the intensity was of the order of 10^{36} erg sec^{-1}. The hardness ratio of 6-10 keV intensity to 2-6 keV intensity of each data for a 10-30 min. interval is plotted against its total intensity, in Fig.21. The hardness ratio inversely correlates with the total intensity in 1984, which is contrast to the positive correlation in 1983. Figure 22 shows the pulse-height spectra in five different intensity levels indicated in Fig.21, where it appeares that a high energy tail grows relatively as the intensity decreases. This may be qualitatively explained by that as an accretion rate decreases down to a level emitting 10^{36} erg sec^{-1}, the emission region on the neutron star surface gradually becomes optically thin. When the emission region is optically thin, the temperature will be much higher than 10^{7} K.

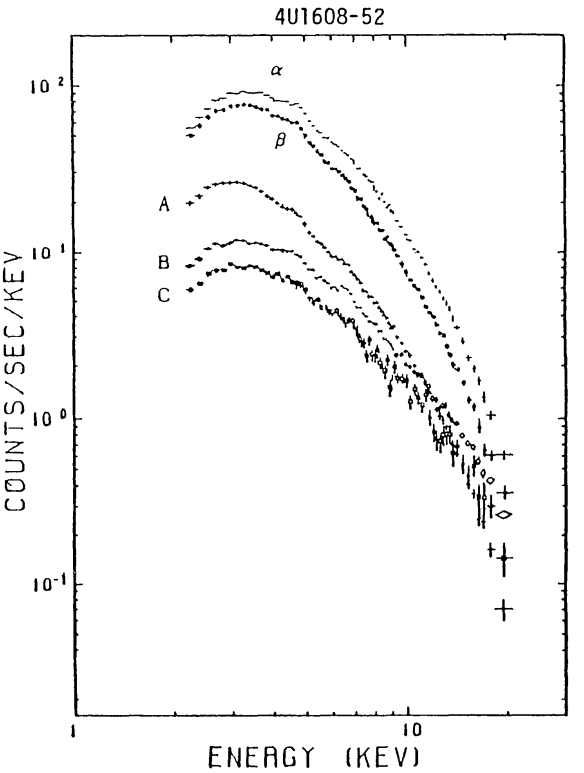

Fig.22 Pulse-height spectra of 4U1608-52 in different periods.

3.5 Ultrasoft Spectra of Black Hole Candidates

Some of low-mass binary sources reveal ultrasoft spectra with a possible hard tail. White and Marshall (1984) point out that these sources are to be investigated for the specific features associated with black hole candidates. The reason is that all sources so far identified as black hole candidates have a state when the spectrum is ultrasoft.

Cyg X-1 has long been known a good black hole candidate (Oda 1977, and references therein). The most convincing basis is the fact that the mass lower limit of the compact object was estimated at 8 $M_\odot$. Cyg X-1 exhibits two distinct states of spectrum; high(soft) and low(hard) states. The low-state spectrum is much softer than those of typical low-mass binary sources. Recently, Cowley et al. (1983) determined the mass function of LMC X-3 which gives a mass lower limit of 7 $M_\odot$. Furthermore, Hutchings et al. (1983) reported that the radial velocity variation of the optical counterpart of LMC X-1 indicates the mass of the compact star to be $\gtrsim$ 3 $M_\odot$. These masses are above the current theoretical limit for the neutron star mass. White and Marshall (1984) shows that the spectra of LMC X-3 and LMC X-1 both have ultrasoft spectra which are similar to the high-state spectrum of Cyg X-1.

GX339-4 and Cir X-1 are also thought to be black hole candidates, although no imformation about the mass of the compact star has been obtained from these sources. These sources undergo bimodal spectral transitions and exhibit rapid intensity variation, similar to Cyg X-1. Figure 23 is the high-state spectrum of GX339-4 observed by Tenma. We can see how the spectrum is soft, by comparing it to those of typical low-mass binary sources in Fig.18.

Since a black hole is generally considered to posses no magnetic field, the accretion disk will extend to near the Schwartzschild radius. The essential difference in the accreting flow to a black hole compared to a neutron star is the absence of a solid surface. Hence, the X-ray emission from an accreting black hole can be understood, at least qualitatively, in terms of the absence of the 2 keV blackbody radiation in

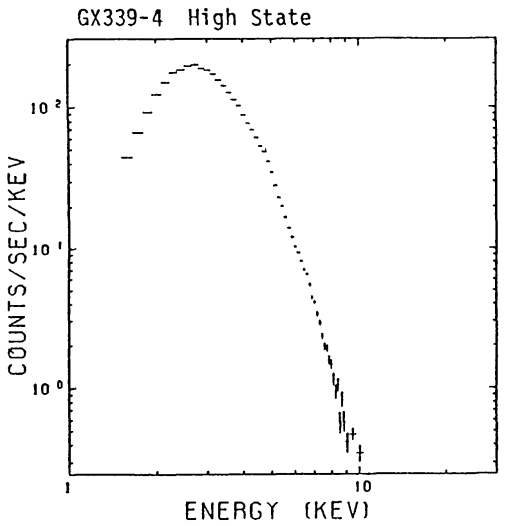

Fig.23 High-state spectrum of GX339-4.

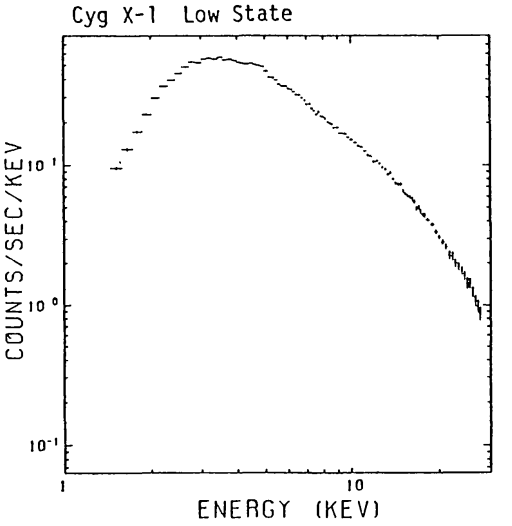

Fig.24 Low-state spectrum of Cyg X-1.

the spectrum from a neutron star source. The accretion disk components decomposed from the spectra of four bright low-mass binary sources in Fig.18 are very much like the high state spectrum of the candidate black hole source.

The ultrasoft spectrum from the candidate black hole source, however, is still softer than the accretion-disk component decomposed from the neutron star source. This can be interpreted by the difference of the mass of the compact object. As discussed before, the optically thick accretion disk in neutron star sources is considered to extend down to near the neutron star surface. On the other hand, the disk in black hole sources has the innermost stable orbit at radius of 3 times of the Schwartzschild radius R_S. Hence, the radius of the inner edge of the disk will have almost the same ratio to R_S for both compact objects. Then, the inner edge temperature of the accretion disk roughly relates with the mass of the compact objects as $T_{in} \propto R_S^{-1/2} \propto M^{-1/2}$ for a constant luminosity. Thus, the lower temperature of the accretion disk will be expected from black hole sources than from neutron star sources, if the mass of the black hole is several times larger than that of the neutron star.

The low-state spectrum lacks the ultrasoft component (see that of Cyg X-1 in Fig.24). A phenomenological picture for the low state is that the inner edge of the optically thick disk recede outward and the Comptonized hard component from the inner optically thin region dominates. Ichimaru (1977) proposed that the transition between the two states of the accretion disk takes place when the accretion rate at the outer boundary of the disk crosses over a critical value. However, why don't usual low-mass binary sources probably containing neutron stars reveal such distinct two states? The presence or absence of the central emission region may also play an important role in triggering the high-low transition.

Most of results discussed above seem to require some modifications for the standard accretion disk model. In particular, the detailed study of the disk properties near compact objects will be very important to find out what are genuine peculiarities revealed by black holes themselves.

REFERENCES

Basko, M.M. 1980, Astron. Astrophys., **87**, 330.
Cowley, A.P. et al. 1983, Astrophys. J., **272**, 118.
Hatchett, S., Buff, J., and McCray, R. 1976, Astrophys. J., **206**, 847.
Hayakawa, S. 1981, Publ. Astron. Soc. Japan, **33**, 365.
Hoshi, R. Publ. Astron. Soc. Japan, **36**, in press.
Hutchings, J.B., Crampton, D., and Cowley, A.P. 1983, Astrophys. J. Letters, **275**, L43.
Ichimaru, S. 1977, Astrophys. J., **214**, 840.
Inoue, H., Koyama, K. et al. 1984, Publ. Astron. Soc. Japan, **36**, in press.
Inoue, H., Waki, I. et al. 1984, Publ. Astron. Soc. Japan, **36**, in press.

Kallman, T.R., and McCray, R. 1982, Astrophys. J. Suppl., **50**, 263.
Kii, T., Nagase, F. et al. 1984, private communication.
Kitamoto, S. et al. 1984, private communication.
Koyama, K. 1984, 'Proc. of the Symposium "X-Ray Astronomy '84", Bologna', in press.
Koyama, K. et al. 1984, Publ. Astron. Soc. Japan, **36**, in press.
Kunieda, H. et al. 1984, Publ. Astron. Soc. Japan, **36**, in press.
Makino, F., Leahy, D.A., and Kawai, N. 1984, this proceedings.
Makishima, K. et al. 1984, in preperation.
Makishima, K., Koyama, K. et al. 1984, private communication.
Milgrom, M. 1976, Astron. Astrophys., **51**, 215.
Mitsuda, K. et al. 1984, Publ. Astron. Soc. Japan, **36**, in press.
Morita, S., and Fijita, J. 1983, J. Phys. Soc. Japan, **52**, 1957.
Nagase, F. et al. 1984, Publ. Astron. Soc. Japan, **36**, in press.
Oda, M. 1977, Space Sci. Rev., **20**, 757.
Ohashi, T. 1981, 'Ph. D. thesis, University of Tokyo' (ISAS RN., **141**).
Ohashi, T. et al. 1984, Publ. Astron. Soc. Japan, **36**, in press.
Pringle, J.E. 1974, Nature, **247**, 21.
Raymond, J.C., and Smith, B.W. 1977, Astrophys. J. Suppl., **35**, 419.
Sato, N., Nagase, F. et al. 1984, private communication.
Suzuki, K. et al. 1984, Publ. Astron. Soc. Japan, **36**, in press.
Tanaka, Y. 1984, this proceedings.
Tarter, C.B., Tucker, W.H., and Salpeter, E.E. 1969, Astrophys. J., **156**, 943.
Tucker, W.H. 1977, Radiation Processes in Astropysics (MIT Press, Cambridge), p.218.
White, N., and Marshall, F.E. 1984, Astrophys. J., **281**, 354.